Journal of Environmental Radioactivity 102 (2011) 620–629

Contents lists available at ScienceDirect

Journal of Environmental Radioactivity

journal homepage: www.elsevier.com/locate/jenvrad

Activity concentrations and dose rates from decorative granite countertops

W.J. Llope*

Rice University, 6100 S. Main St. - MS-315, Houston, TX 77005, United States

ARTICLE INFO

Article history:
Received 21 November 2010
Received in revised form
22 February 2011
Accepted 19 March 2011
Available online 19 April 2011

Keywords:
Granite
Gamma radiation
Dose
Human phantom

ABSTRACT

The gamma radiation emitted from a variety of commercial decorative granites available for use in U.S. homes has been measured with portable survey meters as well as an NaI(Th) gamma spectrometer. The ^{40}K, U-nat, and ^{232}Th activity concentrations were determined using a full-spectrum analysis. The dose rates that would result from two different arrangements of decorative granite slabs as countertops were explored in simulations involving an adult anthropomorphic phantom.

1. Introduction

Thousands of varieties of igneous rocks, marketed generically as "granite," are widely used in U.S. homes as large-area countertops in kitchens and other rooms. These stones can contain admixtures of ^{40}K and the decay series of U-nat and ^{232}Th. These can include a number of progeny radioisotopes that emit gamma rays with characteristic intensities and energies ranging from some tens of keV to ~2.6 MeV. The use of such decorative granites as building materials in a home can thus result in the long-term whole-body exposure of the occupants to this radiation.

Numerous works (Abbady et al., 2005; Abdel Hady et al., 1994; El Afifi, 2006; Al-Jarallah, 2001; Al-Jarallah et al., 2005; Arafa, 2004; Asghar et al., 2008; Badhan et al., 2009; Canbaz et al., 2010; El-Amri et al., 2003; Fazal-ur-Rehman et al., 2003; Fokianos et al., 2007; Haquin, 2008; Iqbal et al., 2000; Kitto et al., 2009; Myatt et al., 2010; Mustonen, 1985a,b; Ningappa et al., 2008; Osmanlioglou, 2006; Pavlidou et al., 2006; Rahman et al., 2008; Petropoulos et al., 2002; Quindos et al., 1988; Sahoo et al., 2007; Al-Selah and Al-Berzan, 2007; Sengupta et al., 2009; Sonkawade et al., 2008; El-Taher et al., 2007; Tzortzis et al., 2003; Walley El-Dine et al., 2001; Xinwei, 2006; Yang et al., 2005) have quantified the ^{40}K, U-nat, and ^{232}Th activity concentrations, in Bq/kg, in specific stones and other building materials. In order to estimate the health risks, these studies commonly provide the values of various hazard indices (Beretka and Matthew, 1985; Malanca et al., 1993; Hayumbu et al., 1995), and/or the dose rates at a distance above a large area of the material using the UNSCEAR scale factors (Beck, 1972; Kohshi et al., 2001; UNSCEAR, 1988; UNSCEAR, 1993; UNSCEAR, 2000), in (nGy/hr)/(Bq/kg). Such dose rate calculations do not seem appropriate for the geometry of a person standing next to a horizontal decorative granite surface. Such dose estimates also tacitly assume that the radioisotope concentrations are uniform throughout the volume of the stone. This assumption can fail for some "exotic" granites, which might exhibit significant "hot spots" within an overall less radioactive bulk volume (Myatt et al., 2010). The use of such dose calculations following the spectroscopic measurements of small samples that happen to include such localized hot spots would thus lead to significant overestimates of the dose.

In this paper, the ^{40}K, U-nat, and ^{232}Th activity concentrations in a number of decorative granite samples marketed to homeowners in the U.S. were measured using an NaI(Tl) gamma spectrometer. The activities were extracted by a full spectrum analysis (Hendriks et al., 2001), and the GEANT4 toolkit was used for the detector efficiency, gamma conversion, and self-absorption corrections (Agostinelli et al., 2003; Barca et al., 2003). The measured activity concentrations were correlated with measurements made using portable survey meters at the surface of the same stones. Some samples studied here did indeed exhibit significant hot spots within a relatively less active overall volume. The dose rates to an adult standing near two different arrangements of decorative granite countertops were explored in GEANT4 simulations

* Tel.: +1 7132564671; fax: +1 7133485215.
E-mail address: llope@rice.edu.

0265-931X/$ – see front matter © 2011 Elsevier Ltd. All rights reserved.
doi:10.1016/j.jenvrad.2011.03.012

including an anthropomorphic phantom. Uniformly active stones, and those with significant hot spots, were treated separately. A similar study using different samples and different methodologies can be found in Ref. (Myatt et al., 2010).

This paper is organized as follows. The experimental aspects are discussed in Section 2. The survey meter results are described in Section 3.1, the activity concentrations obtained from spectroscopy are described in Section 3.2, and the dose rate results are discussed in Section 3.3. The dose rates from the majority of the samples, which indicate relatively low and uniform activity concentrations, are discussed in Section 3.3.1, while the dose rates for the stones which exhibit significant hot spots are discussed in Section 3.3.2. The summary and conclusions are presented in Section 4.

2. Experimental aspects

2.1. Samples and measurements

The decorative granite samples were collected from local natural stone retailers as showroom samples in two batches over the course of ~2 years. These initial sample blocks ranged in size from 5 cm × 5 cm to ~60 cm × 30 cm. Core samples with a diameter of 5 cm were cut from a number of locations per initial block from the first-batch samples. These core samples were measured with an NaI(Tl) spectrometer and two different portable survey meters. The second batch of initial samples was not cored and was measured only with the one of the survey meters. In the following, the 5 cm-diameter core samples from the initial batch of blocks will be referred to as "cores," while the uncored second batch of samples will be referred to as "blocks."

The locations on a sample from which the cores were removed were randomly chosen for stones with uniform color patterns, and were distributed randomly within the different color domains for stones with more varied color patterns. For the NaI(Tl) spectrum measurements, sixty-nine core samples were available from twenty-five different stone types. Each core was two inches in diameter with a sample-to-sample variation in diameter of approximately 2 mm (1/16th inch). The thickness of each core was within a few millimeters of one of three values - 1 cm, 2 cm, or 3 cm. The majority of the samples were 2 cm thick.

The survey meters were a Ludlum[1] Model 14C with Model 44-9 probe and a PalmRAD[2] Model 907. Both are halogen-quenched Geiger-Müller detectors with a circular 45 mm^2 active areas. The survey meter data was collected at the surface of a core or block in the "slow" response mode (20 s averaging). The background count rates were typically 20 counts per minute (CPM).

The NaI(Tl) crystal was 7.6 cm (3 inches) in diameter and 7.6 cm (3 inches) deep. It had a special thin entrance window and was read out by a photomultiplier tube (PMT). The detector was surrounded on all sides by 5 cm-thick Pb blocks. Each core was placed coaxially with the crystal at a distance of 3 mm. The signals from the attached photomultiplier tube were preamplified (Ortec model 113), amplified (Ortec model 485), and then digitized by a 12 bit multi-channel analyzer (MCA). The energy lower limit was 0.1–0.2 MeV and the upper limit was 2.8–2.9 MeV. The energy window used for all of the data analyses was 0.25–2.75 MeV. The data for each core was collected over periods ranging from 2 to 14 h depending on the apparent activity of the core. In between each measurement of a core, data was collected with a ^{22}Na calibration source to set the MCA energy scale. This treated the slow variations in the PMT output (gain) and the temperature dependence of the NaI(Tl) light output. The energy resolution in percent was observed to be $\sigma_E/E = 1.8 + 2/\sqrt{E}$, which corresponded to a full width at half-maximum of 8.5% at 1 MeV.

The background spectra were measured over 14–16 h periods and were remeasured every few weeks. These spectra were consistent in spectral shape and magnitude to ~3% in the different background runs. The experimental spectrum from a core run and a background run were each normalized by the run time, and then subtracted to produce the spectrum from the core in counts per second per 0.02 MeV-wide bin.

A few cores were measured multiple times in order to check the reproducibility and the long-term stability of the results. Some of these measurements of the same core were separated by more than one year of real time. The ^{40}K, U-nat, and ^{232}Th spectral shapes and extracted activity concentrations were always in agreement to better than 10%.

Table 1
The number of different gamma energies, and the average number of gammas per decay of the parent, obtained from the spectra listed in Ref. (Evans, 1983).

Parent	No. of lines	$\langle N_{\gamma/DK} \rangle$
^{40}K	1	0.107
U-nat	84	2.41
^{232}Th	100	4.13

2.2. Simulations & analysis

The detector efficiencies were treated using simulations based on GEANT4 (Agostinelli et al., 2003; Barca et al., 2003). GEANT4 is an object-oriented toolkit for simulating the passage of particles through arbitrary matter arranged in arbitrary geometries. It exists as open-source C++ code and includes all of the necessary functionality for microscopic Monte Carlo simulations including particle tracking through user-defined media including particle decays and the generation of secondary particles from all possible physical interaction processes, the digitization of energy deposition in sensitive volumes ("hits"), and visualization. The analysis and the plotting of the experimentally-measured spectra and the results from the GEANT4 simulations were performed using ROOT (Brun and Rademakers, 1997), which is also freely available. GEANT4 version 9.4 and ROOT version 5.26.00 were used here.

In GEANT4, one gamma per event was emitted into 4π and randomly within a 5 cm diameter by 5 cm thick "test core" that represents the cores that were experimentally measured. The energy of each gamma emitted from this test core was sampled randomly from the full-spectrum[3] (Evans, 1983) for a given parent nucleus - ^{40}K, U-nat, or ^{232}Th. The number of gamma lines, and the average number of gammas emitted per decay of the parent obtained by integrating the spectra, are summarized in Table 1.

Each parent was simulated separately. An NaI(Tl) "test crystal" was also defined in the simulation coaxially with the test core at a separation of 3 mm consistent with the experimental measurements. The energy deposited in the test crystal was smeared event by event with the experimental energy resolution function described above. Granite material was defined in the simulation using the world-wide average density (2.7 g/cm^3) and chemical composition obtained from Ref. (Blatt and Tracy, 1997). Thus, gamma conversion and self-absorption are treated. The three separate sets of simulations thus resulted in three simulated spectra, one each from ^{40}K and the decay series of U-nat and ^{232}Th.

[1] Ludlum Measurements, Inc., 501 Oak Street, Sweetwater, TX 79556 USA.

[2] Berkeley Nucleonics Corporation, 2955 Kerner Blvd. Suite D, San Rafael, CA 94901 USA.

[3] All gamma lines with intensities greater than 0.1 gamma rays per 100 disintegrations of the parent nucleus were included.

To extract the activity concentration for each experimentally-measured core spectrum, a Full Spectrum Analysis (FSA) (Hendriks et al., 2001) was performed. Such an approach is less-sensitive to the uncertainties in spectral stripping analyses (Chiozzi et al., 2000; Løvborg et al., 1979; Rybach, 1971, 1988; Sanzelle et al., 1988) resulting from the choices of the energy windows and the evaluation of the contributions from gammas from other radionuclides in a given window. Small gain variations during long runs of relatively inactive samples can smear the experimental spectra beyond that described by the reference spectra. This minor smearing was indeed observed for the least active samples (see below). To perform the FSA, each of the three GEANT4 -simulated spectra for ^{40}K, U-nat, and ^{232}Th were first normalized to the total number of gammas emitted at the test core (one per "event"). Three scale factors, C_i, were then extracted by regression (χ^2 minimization) to the experimentally-measured spectrum by the fitting procedures built into ROOT. As the experimentally-measured spectra were normalized to the run time in seconds, these scale factors for each core represented the number of measured gammas from each parent per second. The activity concentration for each core in Bq/kg was then calculated using,

$$A_i^k = C_i^k \Big/ \left[\left\langle N^i_{\gamma/DK}\right\rangle * M_k\right], \quad (1)$$

where k was the core-identifying index, $\langle N^i_{\gamma/DK}\rangle$ is given in Table 1, and M_k was the core mass in kg. A similar procedure for normalizing simulated spectra for the extraction of fully efficiency-corrected activity concentrations from experimentally measured spectra is described in Ref. (Hendriks et al., 2002).

A typical example of the full-spectrum fitting result is shown in Fig. 1. The experimentally measured spectrum for this core is shown with the solid points. The simulated spectra are shown with the different line styles: ^{40}K (dot dot dashed), U-nat (dot dashed), and ^{232}Th (dashed). The sum of the simulated spectra is shown as the solid line. The lower frame depicts the fractional difference between the experimental and the sum of the simulated spectra in each 0.02 MeV-wide bin. While the experimental spectrum extends over three orders of magnitude versus the energy, the total spectrum determined by the fitting procedure reasonably reproduces the experimental spectrum in magnitude and shape. The projection of the lower frame of Fig. 1 on the vertical axis is approximately Gaussian in shape with a standard deviation of 9%. This same standard deviation ranges from 7% to 13% for all of the present measurements. The discrepancy for some energy bins in the lower frame of Fig. 1, *e.g.* near ~0.6 MeV, was not uncommon for such a (relatively quiet) core and resulted from the gain variations in the long runs of quiet samples discussed above. The bulk of the spectrum was, however, reasonably reproduced leading to reliable measurements of the activity concentrations.

The minimum detectable activities (MDA) from the present approach were investigated in the following manner. A simulated spectrum for a given parent radionuclide was scaled to an arbitrary test activity and then added to an experimentally measured background spectrum. This sum spectrum was then processed as usual, but the background spectrum taken at another time was used. The resulting "signal" spectrum was then fit using the standard procedure, and the apparent activity concentration was compared to the test value. This was done for each parent and for a number of different combinations of background spectra. The overall results were consistent and implied that the MDA values are approximately 400:80:40 Bq/kg for the ^{40}K:U-nat:^{232}Th parents.

In the same simulations used to treat the NaI(Tl) detector efficiencies (described above), the so-called "MIRD phantom" (Guatelli et al., 2006; Guerrieri, 2005; de Souza e Silva et al., 2009) and one of two different arrangements of decorative granite slabs arranged as

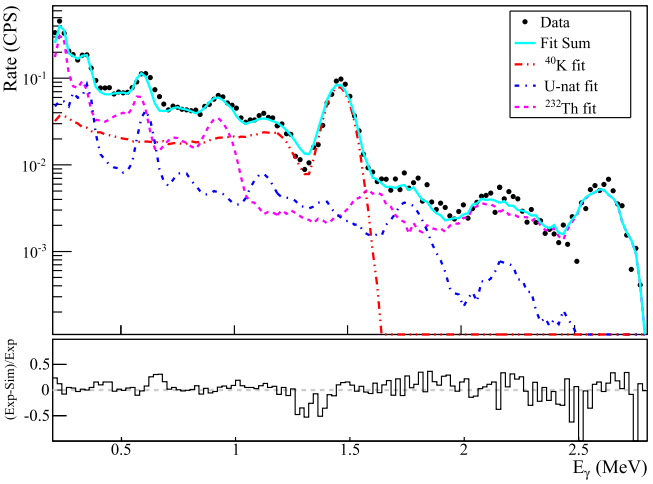

Fig. 1. A typical example of the result from the full-spectrum fitting procedure.

countertops were placed in the same simulation volume.[4] The MIRD anthropomorphic phantom is available as part the standard GEANT4 software distribution. This implementation uses basic geometrical shapes to simulate an adult body both in dimension and chemical composition. In the language of GEANT4, the phantom's thirty-three internal organs are effectively active detectors, and the energies deposited in each of these organs are recorded in a simulation run. The various organs are composed of soft tissue (density ρ = 0.987 g/cm^3, radiation length X_0 = 38.1 cm), bone (ρ = 1.487 g/cm^3, X_0 = 21.4 cm), lung tissue (ρ = 0.296 g/cm^3, X_0 = 123.4 cm), adipose (ρ = 0.93 g/cm^3, X_0 = 44.6 cm) glandular material (ρ = 1.04 g/cm^3, X_0 = 35.8 cm) and breast material (ρ = 0.985 g/cm^3, X_0 = 39.9 cm). The female version of the MIRD phantom was used. The male MIRD phantom has the same overall and organ dimensions and differs from the female version only in the definition of the sexual organs. The MIRD phantom weighs 70 kg (154 pounds), and is approximately 170 cm (68 inches) tall, 40 cm (16 inches) wide, and 23 cm (9 inches) deep.

The two countertop geometries used are depicted in Fig. 2. On the left is a simple "L"-shaped arrangement such as might be found in a workroom, and on the right is an arrangement with a different L-shaped surface, a 6″-tall and 1 cm-thick backsplash, and a detached "island," such as might be found in a home kitchen. The total area of the two geometries is nearly the same – 6 m^2 for the workroom, and 6.1 m^2 for the kitchen (~65 ft^2). For each countertop arrangement, simulations were performed with the phantom placed at the three different locations indicated in each figure. Location "A" is the geometric center of the geometry, location "B" is close to the elbow of the "L", while location "C" is close to, and at the midpoint of, the longer surface.

In each event (for which one gamma was emitted into 4π from the test core in front of the test crystal), a larger number of gammas are emitted into 4π from random locations inside the granite countertops. The number of gammas emitted per event from the countertops was set by the total surface area of countertops divided by the surface area of the core (π [2.5 cm]^2). The total energy deposited in the MIRD phantom was incremented in each event and at the end normalized to the number of events for each simulation. The scale factors, C_i, determined from the full-spectrum

[4] Track-terminating pseudovolumes surrounding the NaI test crystal were used to ensure that there was no "cross talk" between the two types of simulations occurring in parallel.

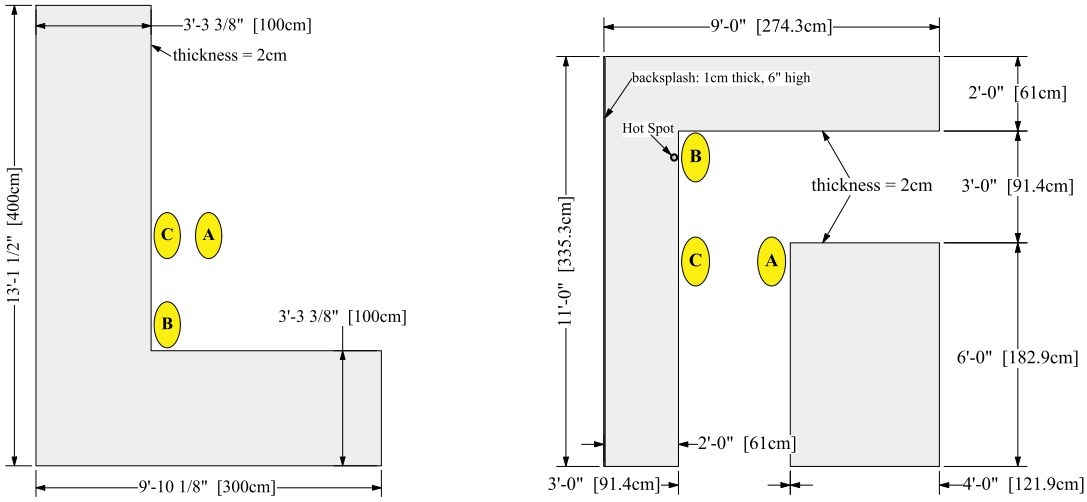

Fig. 2. On the left is the workroom geometry, and on the right is the kitchen geometry. The locations at which the phantom was placed to calculate the dose rates in each of these two geometries are indicated by the ellipses.

analysis of each core were then used to scale the dose to the phantom to units of MeV/s. The energy deposited in the whole phantom and each of the 33 separate body parts was incremented separately. The whole-phantom energy deposition rates were then converted to equivalent dose rates in mSv/s using the appropriate factors and the phantom's total mass.

It is important to note that the scaling described above to determine the dose rates in the phantom that would be obtained from a given experimentally-measured core tacitly assumed that the (small) core had activity concentrations that were representative of those in a much larger slab of the same granite. As will be shown in the next section, some decorative granites showed significant "hot spots" in an otherwise less radioactive overall volume. Special simulations were used to estimate the dose to the phantom for granite slabs that had such hot spots. For these simulations, the location of a hot spot is indicated for the "kitchen" geometry on the right side of Fig. 2. This is a 2.5 cm diameter spot that is 1 cm from the edge of the granite surface and centered on the phantom when in position "B" of the kitchen geometry. This hot spot location thus provides "worst-case" estimates of the dose rates to a human.

2.3. Dose calculation cross-checks

The dose rates determined using the present GEANT4 and the MIRD phantom approach (G4&P) were compared to those from two other approaches to assess the accuracy of the present calculations. In the first approach, the phantom was placed at the center of a room with concrete walls with specific activity concentrations and compared to the results from the "attenuation & buildup" (A&B) approach described by Markkanen et al. (Markkanen, 1995, 1999). In the second approach, an isotropic point source was placed at specific positions in front of the phantom and compared to the results from the software package "VMC-DC " (VMC) (Hunt et al., 2004). The results from these two comparisons are now described in turn.

2.3.1. Comparison to the attenuation & buildup approach

In the A&B approach, the numerical integration of analytical functions with tabulated parameters is performed for a rectangular source of uniform density and activity concentration. Six such rectangular sources are arranged as the walls, floor and ceiling of a room. Attenuation of the photons in the concrete walls and air is

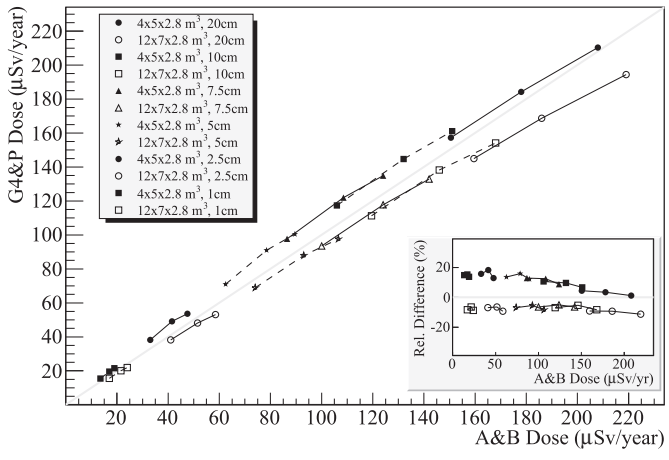

Fig. 3. The comparison of the dose rates obtained from the A&B approach and the GEANT4 approach for various room sizes and wall thicknesses and an exposure of 7000 h. The solid symbols correspond to the smaller room, while the open symbols correspond to the larger room. The inset depicts the relative differences in percent.

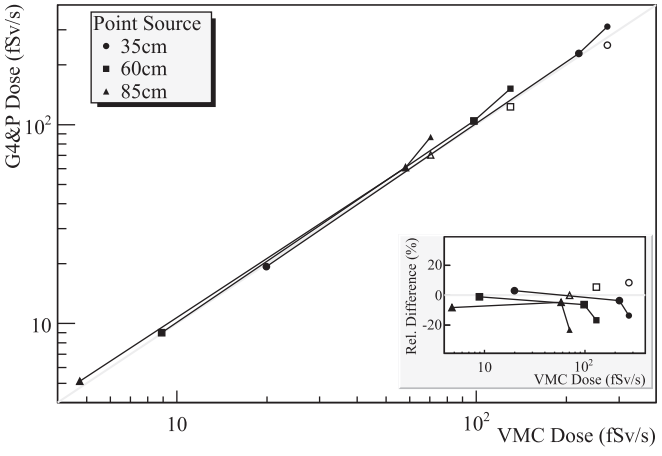

Fig. 4. The comparison of the dose per second for a 1 kBq/s point source obtained from the VMC-DC program and the GEANT4 approach. The solid symbols correspond to the use of the full energy spectrum in the G4&P simulations, while the open symbols correspond to the use of the same simplified energy spectrum for ^{232}Th as is used in the VMC-DC program. The inset depicts the relative differences.

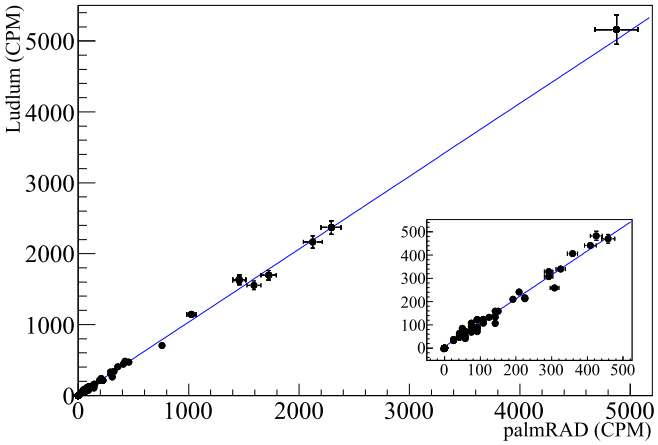

Fig. 5. The correlation of the rates in CPM measured by the Ludlum and palmRad portable survey meters.

treated via tabulated linear attenuation and energy attenuation coefficients, respectively. Buildup is treated via a phenomenological approach (Berger, 1957) also using tabulated parameters (Trubey, 1966; Takeuchi and Shun-ichi, 1985). The sum over the six planes of the effective doses in air in Gy is then multiplied by an overall factor of 0.7 Sv/Gy (Beck, 1972; Kohshi et al., 2001; UNSCEAR, 1988; UNSCEAR, 1993; UNSCEAR, 2000) to obtain the absorbed dose rate to an adult human. This is then scaled to a dose rate per year of exposure using an occupancy factor of 0.8, or 1 year is equal to 7000 h.

Implementations of the original approach of Refs. (Koblinger, 1978; Stranden, 1979; Mustonen, 1985a,b) have been developed with slightly different assumptions in Fortran Markkanen, 1995; Markkanen, 1999; Mirza et al., 1991; Ahmad et al., 1998; Máduar and Hiromoto, 2004), Maple (Ademola and Farai, 2005), and Pascal (Allam, 2009). Overviews of the different approaches and direct comparisons of their results are available in Refs. (Markkanen, 1995; Markkanen, 1999; Ahmad et al., 1998; Máduar and Hiromoto, 2004; Allam, 2009; Risica et al., 2001). Generally, the predictions from the different A&B approaches are consistent to the 10–15% level.

The A&B code used here is the Fortran program MATERIA (Markkanen, 1995, 1999) as the source code was freely available in Ref. (Markkanen, 1995). In the MATERIA code, the ^{40}K, ^{238}U, and ^{232}Th gamma energies and weights are not the complete spectra but are simplified to just one, or in the case of ^{232}Th two, gamma lines with an energy that is a weighted average over the spectrum.

To make a strict comparison to the A&B approach, the present GEANT4 code was extended in the following ways. The granite countertops were removed, and concrete walls as well as a concrete ceiling and floor of specific dimensions were defined. The density and elemental composition of the concrete were taken from Ref. (ICRU, 1989). The MIRD phantom was placed in the center of the room. In the GEANT4 event loop, gammas were emitted into 4π from random locations inside the walls. Every generated photon was emitted with an energy sampled from the full spectrum for ^{40}K, U-nat, or ^{232}Th separately. In each simulation (for a specific room geometry and parent), the total number of emitted gammas, N_i^{γ}, was typically in the range of 5–10 million. The direct comparison of the G4&P doses to those from the A&B approach required a temporal scaling which was accomplished as follows. The total activity for each decay series and room geometry, A_i^{tot} in Bq, was given by $A_i \times \rho \times V_{walls,}$ where ρ was the density of the concrete in kg/m^3, and V_{walls} was the total wall, floor, and ceiling volume in m^3. The ^{40}K, U-nat, and ^{232}Th activity concentrations were arbitrarily set to $A_K = 400$ Bq/kg, $A_U = 40$ Bq/kg, and $A_{Th} = 40$ Bq/kg, respectively, in both codes. The temporal scale factor in s^{-1} for a given input activity concentration, A_i in Bq/kg, was then given by $[A_i\,(\mathrm{Bq/kg})] \times [\rho\,(\mathrm{kg/m^3})] \times [V_{walls}\,(\mathrm{m^3})]/\langle N^i_{\gamma/DK}\rangle$, where $\langle N^i_{\gamma/DK}\rangle$ is given in Table 1. The product of the G4&P-calculated doses, in mSv, and these scale factors thus gave the dose rates in mSv/s. These dose rates were then multiplied by the total time interval of 7000 h.

The comparison of the dose rates obtained from the A&B approach and the G4&P approach are depicted in Fig. 3. Two different room sizes, 5 m × 4 m × 2.8 m (solid points) and 12 m × 7 m × 2.8 m (open points), and a number of different wall thicknesses, were used. While the A&B approach is deterministic, based on analytical functions with tabulated parameters, and uses a simplified set of gamma intensities and energies, and the G4&P approach is a full-physics Monte Carlo using an adult anthropomorphic phantom with the complete gamma emission spectra, the agreement between the two is reasonable over a factor >10 range in the absorbed doses. The inset depicts the relative difference (G4&P − A&B)/A&B in percent. For the smaller room, the G4&P results are larger than the A&B results by ∼18% for the thinnest walls and approach the A&B results as the wall thickness increases. For the larger room, the G4&P results are consistently 10–15% smaller than the A&B results. Nonetheless, the two approaches are consistent over a wide range of room geometries.

2.3.2. Comparison to the VMC approach

The computer program VMC-DC (Hunt et al., 2004) is freely available and allows the calculation of dose rates from geometrically

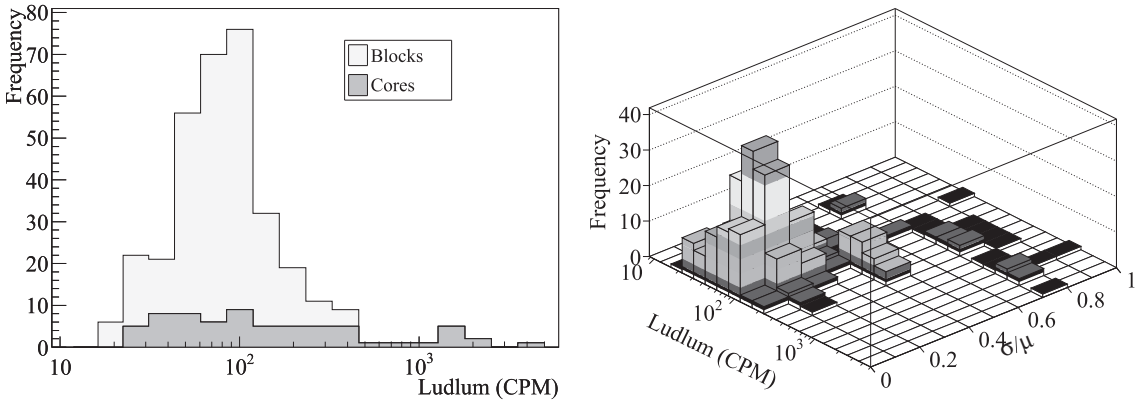

Fig. 6. On the left is the frequency distribution of the Ludlum survey meter readings in CPM. The values for the cores and the values from scans across the surface of the blocks, are shown separately as the two stacked histograms as labelled. On the right is the two-dimensional frequency distribution for the cores and blocks versus the Ludlum survey meter reading and the standard deviation divided by the mean determined for each initial block separately.

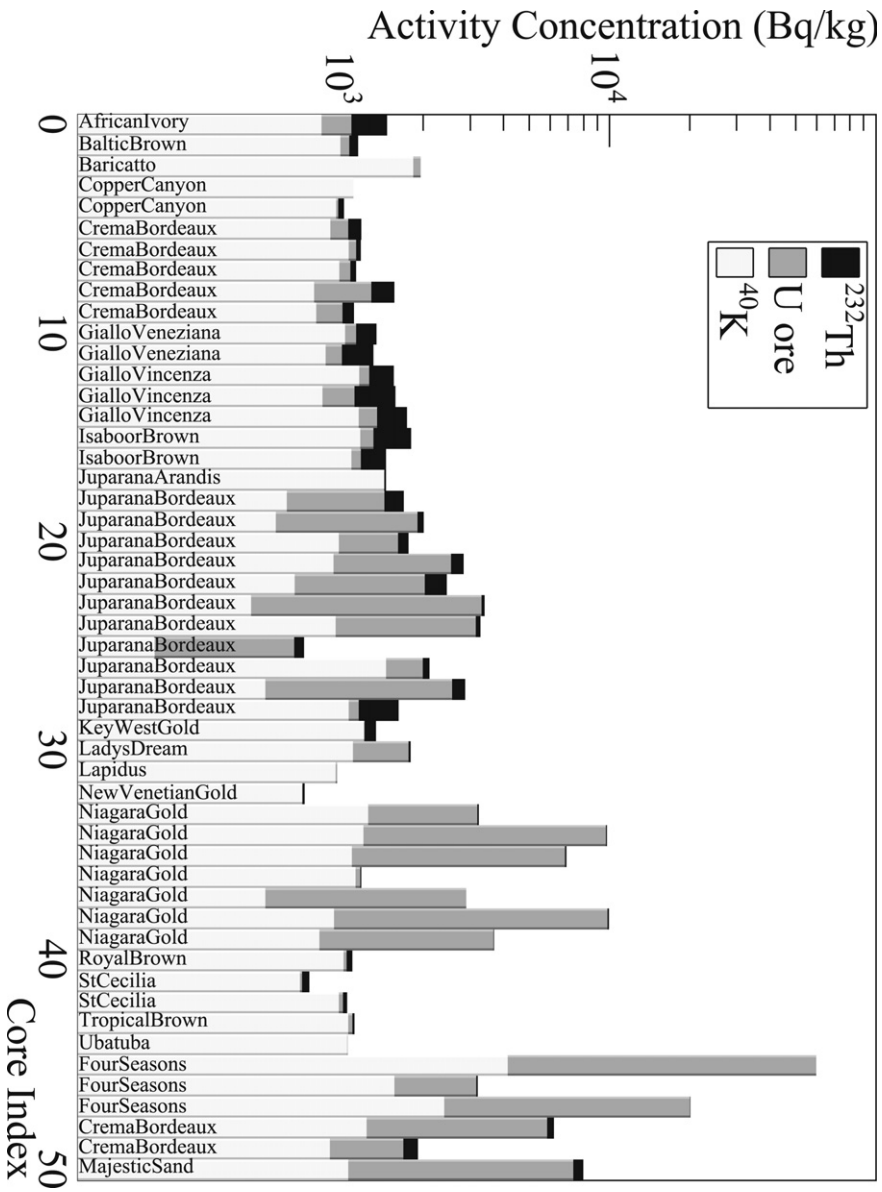

Fig. 7. The ^{40}K, U-nat, and ^{232}Th activity concentrations for the different cores.

simple sources. The program includes the so-called Yale voxelized phantom (Zubal et al., 1994), which was based on magnetic resonance images of a human male. The outer dimensions of the Yale phantom are very similar to those of the MIRD phantom, but the shapes of the organs are no longer simple geometrical shapes. The VMC-DC program was run for a point source 1 m above the ground at horizontal distances from the central axis of the Yale phantom of 35, 60, and 85 cm. Ten million histories were run separately for 1 kBq/s ^{40}K, U-nat, and ^{232}Th sources, and at the end the program reported a total effective dose in fSv. The VMC-DC program uses a shorter list of gamma energies and weights than does the G4&P simulations - only those gammas with intensities above 1% and energies above 18 keV were included. The present G4&P code was modified to include a point source at the same three positions, and $N_i^{\gamma} = 100000$ gammas were generated for each parent, *i*. The assumption of 1 kBq/s used in the VMC-DC program then gave the effective time interval for each G4&P simulation as 970.9, 41.5, and 24.3 s, respectively. The total dose from the G4&P simulation of 100000 gammas was then divided by these time intervals to give the total dose per second.

The comparison of the dose per second obtained from the G4&P and VMC approaches is depicted in Fig. 4. The different point styles correspond to the different distances between the point source and the central axis of the phantom. Each connected group of three symbols indicates the dose from ^{40}K, U-nat, and ^{232}Th going from left to right, respectively. The inset depicts the relative difference (G4&P − VMC)/VMC in percent. This figure indicates that the G4&P simulation is consistent with the VMC-DC program to better that 10% for the ^{40}K and U-nat components. However, the ^{232}Th component consistently results in a ∼20% higher dose in the G4&P simulations compared to the VMC-DC result. This discrepancy is the result of the simplified energy spectrum used in the VMC-DC code, which ignores a number of relatively high energy emission lines because their activity is less than 1%. The use of the same simplified ^{232}Th spectrum in the G4&P simulations results in the open points in Fig. 4. With the now more consistently defined ^{232}Th spectra, the dose rates from the G4&P and VMC-DC codes agree to better than 10% for all three components over a range of ∼2 orders of magnitude.

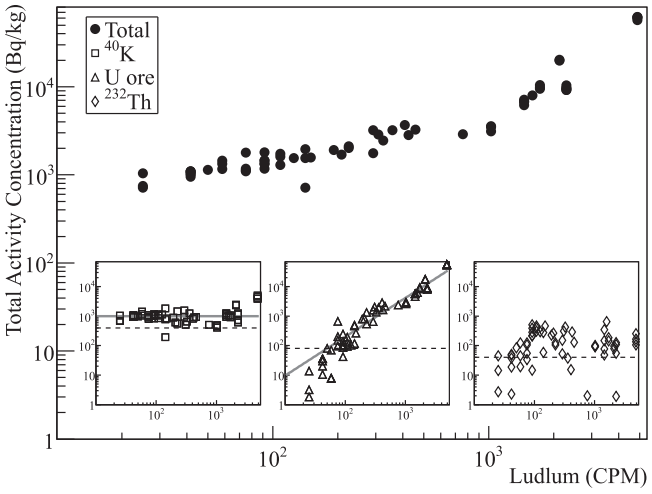

Fig. 8. The correlation of the rates measured by the Ludlum survey meter to the activity concentrations determined from the full-spectrum analyses of the measured NaI(Tl) spectra. The dashed horizontal lines in each inset depict the minimum detectable activities for each decay series.

3. Results

3.1. Survey meter measurements

The correlation of the rates per minute measured by the Ludlum and palmRad portable survey meters at the surface of each core is shown in Fig. 5. The results from the two different survey meters are consistent. The majority of the cores have count rates that are less than 200 CPM. A smaller number of cores have significantly higher rates.

Shown on the left side of Fig. 6 is the frequency distribution of the Ludlum survey meter readings in CPM. The values for the cores, and the results from scanning over the surface of the blocks, are shown as the two stacked histograms. The most probable survey meter reading was ∼100 CPM. The values from the cores taken from the same initial sample, and by scanning across the surface of the (uncored) blocks, were used to define a mean value and standard deviation of the survey meter readings from each stone sample. Shown on the right side of Fig. 6 is the two-dimensional frequency distribution of the Ludlum survey meter reading (for a core, or a location on a block) and the standard deviation divided by the mean determined for each sample separately. This figure implies that the stones that are relatively inactive are uniformly inactive, while the highest survey meter readings result from "hot spots" in otherwise relatively inactive stones. This observation plays an important role in the determination of the dose rates to be expected from decorative granites that was described in Section 3.3. According to this figure, stones with survey meter readings below ∼200 CPM are considered to be "uniformly active" to approximately the ∼30% level.

Table 2
The dose rates assuming the countertops are either a uniformly-active 1 kBq/kg ^{40}K source or a uniformly active source of 1 kBq/kg ^{40}K, 50 Bq/kg U-nat, and 50 Bq/kg ^{232}Th.

Geometry	Position	Dose rate (μSv/yr) ^{40}K only, 1 kBq/s	Dose rate (μSv/yr) mixture
Workroom	A	1.0	2.3
	B	2.1	4.8
	C	1.7	3.8
Kitchen	A	1.4	3.1
	B	1.9	4.5
	C	1.7	3.8

3.2. Activity concentrations

The ^{40}K, U-nat, and ^{232}Th activity concentrations extracted from the FSA of each core are depicted in Fig. 7. The commercial trade names for each core labelled are in the figure. The ^{40}K activity concentration was rather uniform across the different cores with mean value of 990 Bq/kg and a standard deviation of 206 Bq/kg. The largest ^{40}K activity concentration observed was 4.1 kBq/kg from a core of "Four Seasons." The U-nat and ^{232}Th activity concentrations were more varied across the different cores. The highest activity concentration cores were 55.4 kBq/kg for U-nat (from the same sample of Four Seasons), and 0.65 kBq/kg for ^{232}Th (from "Majestic Sand" *a.k.a.* "Shivakasi").

Activity concentrations from decorative granites imported into various countries for use as building materials have been reported in Refs. (Pavlidou et al., 2006) (Greece), (Tzortzis et al., 2003) (Cyprus), (Al-Selah and Al-Berzan, 2007) (Saudi Arabia), (Kitto et al., 2009) (United States), and (Myatt et al., 2010) (United States). It was generally observed that the ^{40}K activity concentrations were relatively uniform across all samples with values of 1–2 kBq/kg, while the U-nat and ^{232}Th activity concentrations were more varied. The same conclusions are drawn from the present samples.

The correlation of the count rates measured by the Ludlum survey meter to the activity concentrations for each core is shown in Fig. 8. The total activity concentration - the sum of the ^{40}K, U-nat, and ^{232}Th activity concentrations - is shown versus the survey meter reading in CPM as the solid points in the main frame. The total activity concentration rises with the survey meter reading for survey meter values up to ∼1000 CPM, and then increases more rapidly above that point.

The three insets of Fig. 8 depict the correlations between the survey meter measurements and the activity concentration for each of the three decay series separately. The minimum detectable activity for each decay series is shown as the dashed horizontal line in each inset. The ^{40}K activity concentration shown in the left inset is constant up to survey meter values near ∼1000 CPM, above which it rises. A rather strong, power-law, correlation between the U-nat activity concentration and the survey meter readings is seen in the middle inset. Admixtures of ^{232}Th up to ∼1000 Bq/kg are observed for survey meter readings above ∼70 CPM, but the ^{232}Th activity concentration does not show a strong correlation with the survey meter readings. It thus appears to be a reasonable approximation that survey meter readings near and below ∼100 CPM result from nearly pure ^{40}K sources, while the more active cores with survey meter readings above ∼1000 CPM result predominantly from significant admixtures of U-nat.

3.3. Dose rates

The dose rates to an adult human in proximity to a countertop arrangement of decorative granite is discussed in this section. It is important to separate these dose rate calculations according to the variability of the radioactivity over the surface of a large slab of granite. Stones with relatively low activities, *i.e.* below ∼200 CPM according to the survey meter, are uniformly active. However, there are also stones for which significant "hot spots" exist within an overall relatively quieter stone. These two cases are now discussed in turn.

3.3.1. Dose rates from uniform stones

For uniform stones, the dose rates to the phantom were calculated in two different ways. The first method involved the specification of the three activity concentrations and then a temporal scaling of the simulations themselves. The second method used the

Table 3
The slopes of the dose rates versus the survey meter readings in (μSv/yr)/CPM for cores from samples that are uniformly active to the ~30% level.

Geometry	Position	Dose rate slope (μSv/yr)/CPM
Workroom	A	0.064
	B	0.13
	C	0.11
Kitchen	A	0.088
	B	0.13
	C	0.11

temporal scale factors determined from each experimentally measured core that was described in the previous section.

For the first of these approaches, the three activity concentrations were assumed. A simulation run, which was typically a few hundred thousand events, produces a single whole-phantom total dose value for a given decay series, countertop geometry, and phantom location. The total number of parent decays in each simulation run was given by

$$N_{DK} = N_{event} N_{\gamma/evt} / N_{\gamma/DK}, \quad (2)$$

where Nγ/*evt* is the total number of gammas emitted from the countertops per event. The equivalent real-time for each simulation run in seconds was then given by

$$t_{equiv} = N_{DK}/[AM] \quad (3)$$

where A was the assumed activity concentration and M was the total mass of the countertops. The dose rate for each simulation run was then the whole-phantom total dose divided by the equivalent real-time. These dose rates were then per second, and were scaled to one year assuming an exposure of 2 h per day and 300 days per year.

The dose rates in μSv/yr for the two countertop geometries and three phantom positions are listed in Table 2. Two different activity concentrations were assumed - a pure ^{40}K source with an activity of 1 kBq/kg, and a source that is 1 kBq/kg ^{40}K, 50 Bq/kg U-nat, and 50 Bq/kg ^{232}Th. The dose rates in all cases were quite low – <5 μSv/yr (600 h). The dose rates increased as the phantom was moved closer to larger countertop areas in the order A (geometric center of geometry) to C (close to longer surface) to B (close to elbow of the "L"). The dose rates in the workroom geometry approximately doubled when the phantom was moved from position A to position B. The dose rates for position B in the two geometries were approximately equal. These results suggest the importance of the solid-angle effect. The closer the phantom was to the countertops, the larger the dose, or, the larger the area of countertops near the phantom, the larger the dose.

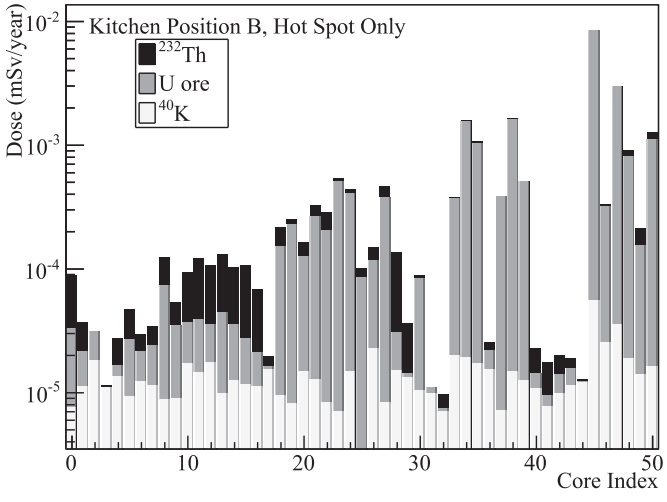

Fig. 9. The dose rates per year (600 h) for each core assuming the phantom is at position B of the kitchen geometry and the core location was at the "hot spot" location indicated in Fig. 2. The rest of the countertop surface in this simulation did not emit gamma rays.

The second approach involved scaling the dose rates from each experimentally measured core using the temporal scale factors from the FSA. As discussed in section 2.2, this approach is only valid for cores that can be considered representative of a larger slab of the same type of granite. As shown in Fig. 8, the activity concentrations measured for each core are generally correlated with the survey meter readings. The slope of these correlations, *i.e.* the dose rate in μSv/yr per CPM (above background) according to the survey meter are listed in Table 3. These slopes range from ~0.06 to 0.13 (μSv/yr)/CPM. The dose rates for the most probable case of a uniform 100 CPM stone range from 6 to 13 μSv/yr depending on the countertop geometry and phantom position. The dose rate for a 200 CPM stone, which is the largest survey meter reading for which the assumption of uniformity still approximately holds, ranges from 12 to 26 μSv/yr.

3.3.2. Dose rates including one hot spot

To investigate the dose rates to be expected for a decorative granite surface including significant hot spots, a 2.5 cm diameter source was defined at the location depicted on the right side of Fig. 2. This source was, at its closest point, 1 cm from the edge of the counter and centered on the phantom when it was in position B. In the GEANT4 event loop, one gamma was emitted into 4π from random locations inside the "test core" in front of the NaI(Tl) detector (as required for the full-spectrum analysis), and, in addition, one gamma was thrown from the hot spot location, also randomly in location and into 4π. No gammas were emitted from the remainder of the countertop surface. This allowed the direct normalization of the dose from any core at this location to the measured spectrum. The granite material was still defined in this simulation even though no gammas were emitted from the majority of the volume, so conversions in the remainder of the granite volume and self-absorption effects were still included.

Shown in Fig. 9 are the dose rates per year (600 h) for each experimentally measured core assuming the phantom was at position B of the kitchen geometry and the core location was at the location indicated on the right side of Fig. 2. The hottest core available, which has a total activity concentration of ~60 kBq/kg, results in a dose rate of only 8 μSv/year.

According to Section 3.3.1, the total dose rate from a uniformly radioactive kitchen geometry of 1 kBq/kg of ^{40}K and phantom position B was 13 μSv/year. Thus, the total dose rate including the hottest core used in this study embedded in this otherwise less radioactive surface was 21 μSv/yr. Isolated hot spots, even if close to the phantom, do not result in significant doses. This is due to the solid-angle effect and significant self-shielding of the radiation by the stone slab itself.

4. Summary and conclusions

Samples of decorative granites were collected from local retailers and measured in several ways. Survey meters were used to measure count rates at the surface, and an NaI(Tl) spectrometer was used to measure the ^{40}K, U-nat, and ^{232}Th activity concentrations. Simulations based on the GEANT4 toolkit and using the MIRD anthropomorphic phantom were used to relate the survey meter and spectroscopic measurements to whole-body dose rates per year (1 yr = 600 h) for an adult standing at several locations near two different horizontal arrangements of the granite as countertops. The reliability of these dose rate simulations was explored by comparing to a "room model" analytical approach as well as an

application that includes simple source geometries and the Yale voxelized phantom.

A relatively strong correlation between the survey meter readings at the surface and the activity concentrations obtained via spectroscopy was observed. The stones with count rates below ~100 CPM were nearly pure ^{40}K sources. The average ^{40}K activity concentration over all cores was approximately constant versus the survey meter reading and had a mean value of 990 Bq/kg with a standard deviation of 206 Bq/kg. A strong power–law relationship between the survey meter readings and the U-nat activity concentration was observed. The hottest cores in this study were predominantly U-nat sources. The ^{232}Th activity concentrations were essentially uncorrelated with the survey meter readings.

The majority of the stones in this analysis were uniformly active and resulted in survey meter readings at the surface of less than 200 CPM above background. These stones were predominantly ^{40}K sources with smaller admixtures (<100 Bq/kg) of U-nat and ^{232}Th. The dose rates for these stones ranged from ~1–~26 μSv/yr depending on the position of the phantom and the countertop geometry. The scale factor relating the whole body dose in μSv/yr to the survey meter reading (in CPM above background) at the surface of these uniform stones was [0.06–0.14 μSv/yr]/CPM. The approximate factor of two range in this slope results from the specific geometry of the decorative granite countertops and the position of the person with respect to these surfaces.

A smaller number of samples indicated significant hot spots embedded in an overall relatively less radioactive stone. The most active core in this analysis, from a stone called “Four Seasons,” resulted in a survey meter reading of 4900 CPM and activity concentrations of 4144 Bq/kg, 55440 Bq/kg, and 140 Bq/kg for the ^{40}K, U-nat, and ^{232}Th series, respectively. This activity concentration is a factor of three larger than the largest total activity concentration from natural stone that has been reported (Arafa, 2004). A 2.5 cm diameter “hot spot” with this activity concentration close to the phantom resulted in a dose rate of only ~8 μSv/yr. Stones called “Juparana Bordeaux,” “Shivakasi,” and “Niagara Gold” also commonly exhibited significant hot spots. Stones with a larger number of hot spots, or larger-area regions of elevated activity concentrations, could result in higher doses. Alternatively, longer exposure times per day, or different phantom arrangements (such as sitting at and/or leaning over the countertop), could also result in higher dose rates. However, the present results indicate that a person standing upright near the most common granite countertops for 2 h per day and 300 days per year receives in whole body doses of only some tens of μSv per year. These values are negligible compared to the natural background and typical regulatory limits.

For the more radioactive cores in this analysis, the activity concentrations obtained are such that the UNSCEAR hazard indices and/or the doses calculated from the activity concentrations and these UNSCEAR scale factors (Beck, 1972; Kohshi et al., 2001; UNSCEAR, 1988; UNSCEAR, 1993; UNSCEAR, 2000) would be very large and thus, *prima facie*, a cause for concern. However, the full simulations imply that such hot spots embedded in a more typically radioactive overall volume result in doses of only some tens of μS/year even if the phantom is very close to the hot spot. This calls into question the use of hazard indices calculated from the spectra obtained from core samples for the prediction of dose rates. A similar conclusion was drawn in Ref. (Myatt et al., 2010).

Acknowledgements

The author wishes to thank Profs. S. Dodds and G.S. Mutchler (deceased), Rice University, Dr. M. Kitto, New York State Department of Health, and Prof. D. Steck, St. Johns University, for numerous productive discussions.

References

Abbady, A.G.E., Uosif, M.A.M., El-Taher, A., 2005. Natural radioactivity and dose assessment for phosphate rocks from Wadi El-Mashash and El-Mahamid Mines, Egypt. J. Environ. Radioactivity 84, 65.
Abdel Hady, E., El-Sayed, A.M.A., Ahmed, A.A., Hussein, A.Z., 1994. Natural radioactivity of basement younger granite rocks from the eastern desert. Radiat. Phys. Chem. 44, 223.
Ademola, J.A., Farai, I.P., 2005. Annual effective dose due to natural radionuclides in building blocks in eight cities of Southwestern Nigeria. Rad. Prot. Dosimetry 114, 524.
Agostinelli, S., et al., 2003. *GEANT4-a simulation toolkit*. Nucl. Instr. Meth. Phys. Res. Sect. A. 506, 250.
Ahmad, N., Hussein, A.J.A., Aslam, 1998. Radiation doses in Jordanian dwellings due to natural radioactivity in construction materials and soil. J. Environ. Radioactivity 41, 127.
Al-Jarallah, M., 2001. Radon exhalation from granites used in Saudi Arabia. J. Environ. Rad. 53, 91.
Al-Jarallah, M.I., Fazal-ur-Rehman, Musazay, M.S., Aksoy, A., 2005. Correlation between radon exhalation and radium content in granite samples used as construction material in Saudi Arabia. Rad. Meas. 40, 625.
Al-Selah, F.S., Al-Berzan, B., 2007. Measurements of natural radioactivity in some kinds of marble and granite used in Riyadh region. J. Nucl. Radiat. Phys. 2, 25.
Allam, K.A., 2009. New model for dwelling dose calculation using Monte Carlo integration. Rad. Prot. Dosimetry 133, 153.
Arafa, W., 2004. Specific activity and hazard of granite samples collected from the Eastern desert of Egypt. J. Environ. Radioactivity 75, 315.
Asghar, M., Tufail, M., Sabiha, J., Abid, A., Waqas, M., 2008. Radiological implications of granite of northern Pakistan. J. Rad. Prot. 28, 387.
Badhan, K., Mehra, R., Sonkawade, R.G., Singh, S., 2009. Use of gamma-ray spectrometry for assessment of natural radioactive dose in some samples of building materials. Asian J. Chem. 21, S207.
Barca, G., et al., 2003. A powerful simulation tool for medical physics applications: GEANT4. Nucl. Phys. B. (Proc. Suppl. 125, 80.
Beck, H.L., et al., 1972. *In-situ Ge(Li) and NaI(Tl) Gamma Ray Spectroscopy Report*, HASL 258. Health and Safety Laboratory, AEC, New York.
Beretka, J., Matthew, P.J., 1985. Natural radioactivity of Australian building materials, industrial wastes and by-products. Health Phys. 48, 87.
Berger, M.J., 1957. Calculation of energy dissipation by gamma radiation near the interface between two media. J. Appl. Phys. 28, 1502.
Blatt, H., Tracy, R.J., 1997. Petrology, second ed.. Freeman, New York, ISBN 0716724383, p. 66.
Brun, R., Rademakers, F., 1997. ROOT - An object oriented data analysis framework. In: Proceedings AIHENP'96 Workshop, Lausanne, 1996. Nucl. Inst. and Meth. in Phys. Res. A, 389, p. 81. available at: http://root.cern.ch/.
Canbaz, B., Füsun Çam, N., Yaprak, G., Candan, O., 2010. Natural radioactivity (^{226}Ra, ^{232}Th and ^{40}K) and assessment of radiological hazards in the Kestanbol granitoid, Turkey. Rad. Prot. Dosimetry 141, 192.
Chiozzi, P., De Felice, P., Fazio, A., Pasquale, V., Verdoya, M., 2000. Laboratory application of NaI(Tl) γ-ray spectrometry to studies of natural radioactivity in geophysics. Appl. Rad. Isot. 53, 127.
El Afifi, E.M., et al., 2006. Evaluation of U, Th, K and Emanated radon in some NORM and TENORM. Rad. Meas. 41, 627.
El-Amri, A., Al-Jarallah, M.I., Abu-Jarad, F., Fazal-ur-Rehman, 2003. Uniformity in radon exhalation from construction materials using can technique. Rad. Meas. 36, 453.
El-Taher, A., Uosif, M.A.M., Orabi, A.A., 2007. Natural radioactivity levels and radiation hazard indices in granite from Aswan to Wadi El-Allaqi southeastern desert, Egypt. Rad. Prot. Dosimetry 124, 148.
Evans, M.L., 1983. Calculation of Terrestrial Gamma-ray Fields in Airborne Radiometric Surveys. Los Alamos National Laboratory. LS-9471-MS.
Fazal-ur-Rehman, Al-Jarallah, M.I., Musazay, M.S., Abu-Jarad, F., 2003. Application of the can technique and radon gas analyzer for radon exhalation measurements. Appl. Rad. Isot. 59, 353.
Fokianos, K., Sarrou, I., Pashalidis, I., 2007. Increased radiation exposure by granite used as natural tiling rock in Cypriot houses. Rad. Meas. 42, 446.
Guatelli, S., et al., 2006. GEANT4 anthropomorphic phantoms. IEEE Nucl. Sci. Symp. Conf. Rec. San Diego.
Guerrieri, G., 2005. Development of anthropomorphic models for radiation protection and radiotherapy, Ph.D. dissertation, Univ. Genoa.
Haquin, G., 2008. Natural Radioactivity and Radon in Building Materials Proc. of 12th Intl. Congress of the Intl. Rad. Prot. Assn., Buenos Aires.
Hayumbu, P., Zaman, M.B., Lubaba, N.C.H., Munsanje, S.S., Nuleya, D., 1995. Natural radioactivity in Zambian building materials collected from Lusaka. J. Radioanal. Nucl. Chem. 199, 229.
Hendriks, P.H.G.M., Limburg, J., de Meijer, R.J., 2001. Full-spectrum analysis of natural γ-ray spectra. J. Environ. Radioactivity 53, 365.
Hendriks, P.H.G.M., Maučec, M., de Meijer, R.J., 2002. MCNP modelling of scintillation-detector γ-ray spectra from natural radionuclides. Appl. Rad. Isot. 57, 449.
Hunt, J.G., da Silva, F.C.A., Mauricio, C.L.P., dos Santos, D.S., 2004. The validation of Voxel phantoms and Monte Carlo methods applied to external irradiations. Rad. Prot. Dosimetry 108, 85–89. see also. http://www.vmcsoftware.com/. J. Hunt, *Visual Monte Carlo*.
ICRU, 1989. Tissue Substitutes in Radiation Dosimetry and Measurement," Report 44 of the International Commission on Radiation Units and Measurements (Bethesda, MD). http://physics.nist.gov/PhysRefData/XrayMassCoef/tab2.html.

Iqbal, M., Tufail, M., Mirza, S.M., 2000. Measurement of natural radioactivity in marble found in Pakistan using a NaI(Tl) gamma-ray spectrometry. J. Environ. Radioactivity 51, 255.
Kitto, M.E., Haines, D.K., Menia, T.A., 2009. Assessment of gamma-ray emissions from natural and manmade decorative stones. J. Radioanal. Nucl. Chem. 282, 409.
Koblinger, L., 1978. Calculation of exposure rate from gamma sources in walls of buildings. Health Phys. 34, 459.
Kohshi, C., Takao, I., Hideo, S., 2001. Terrestrial gamma radiation in Koshi prefecture, Japan. J. Health Sci. 47, 362.
Løvborg, L., Jensen, L.B., Kirkegaard, P., Christiansen, E.M., 1979. Monitoring of natural soil radioactivity with portable gamma spectrometer. Nucl. Inst. Methods 167, 341.
Máduar, M.F., Hiromoto, G., 2004. Evaluation of indoor gamma radiation dose in dwellings. Rad. Prot. Dosimetry 111, 221.
Malanca, A., Passina, V., Dallara, G., 1993. Radionuclide content of building materials and gamma-ray dose rates in dwellings of Rio-Grande Do-Norte Brazil. Rad. Prot. Dosimetry 48, 199.
Markkanen, M., November 1995. "Radiation Dose Assessments for Materials with Elevated Natural Radioactivity," Report STUKBSTO 32, 1995 (Helsinki: Säteilyturvakeskus).
Markkanen, M., 1999. "Radiological Protection Principles Concerning the Natural Radioactivity of Building Materials," Radiation Protection 112. Office for Official Publications of the European Communities, Luxembourg.
Mirza, N.M., Ali, B., Mirza, S.M., Tufail, M., Ahmad, N., 1991. A shape and mesh adaptive computational methodology for gamma ray dose from volumetric sources. Rad. Prot. Dosimetry 38, 307.
Mustonen, R., 1985a. Natural radioactivity in, and radon exhalation from, Finnish building materials. Health Phys. 46, 1195.
Mustonen, R., 1985b. Methods for evaluation of radiation from building materials. Rad. Prot. Dosimetry 7, 235.
Myatt, T.A., Allen, J.G., Minegishi, T., McCarthy, W.B., MacIntosh, D.L., McCarthy, J.F., 2010. Assessing exposure to granite countertops Part 1: radiation. J. Expo. Sci. Environ. Epidemiol. 20, 280.
Ningappa, C., Sannappa, J., Karunakara, N., 2008. Study on radionuclides in granite quarries of Bangalore rural district, Karnataka, India. Rad. Prot. Dosimetry 131, 495.
Osmanlioglou, A.E., 2006. Natural radioactivity and evaluation of effective dose equivalent of granites in Turkey. Rad. Prot. Dosimetry 121, 325.
Pavlidou, S., Koroneos, A., Papastefanou, C., Christofides, G., Stoulos, S., Vavelides, M., 2006. Natural radioactivity of granites used as building materials. J. Environ. Radioact. 89, 48.
Petropoulos, N.P., Anagnostakis, M.J., Simopoulos, S.E., 2002. Photon attenuation, natural radioactivity content and radon exhalation rate of building materials. J. Environ. Radioactivity 61, 257.
Quindos, L.S., Newton, G.J., Fernandez, P.L., Soto, J., 1988. Natural radioactivity of some Spanish building materials. Sci. Tot. Environ. 68, 181.
Rahman, S., Faheem, M., Matiullah, 2008. Natural radioactivity measurements in Pakistan - an overview. J. Rad. Prot. 28, 443.
Risica, S., Bolzan, C., Nuccetelli, C., 2001. Radioactivity in building materials: room model analysis and experimental methods. Sci. Tot. Environ. 272, 119.
Rybach, L., 1971. Modern Methods of Geochemical Analysis. Plenum Press, New York. 271–318.
Rybach, L., 1988. Handbook of Terrestrial Heat-Flow Density Determination. Kluwer Academic Publishers, Dordrecht, pp. 125–142.
Sahoo, B.K., Nathwani, D., Eappen, K.P., Ramachandran, T.V., Gaware, J.J., Mayya, Y.S., 2007. Estimation of radon emanation factor in Indian building materials. Rad. Meas. 42, 1422.
Sanzelle, S., Erramli, H., Fain, J., Miallier, D., 1988. The assessment of gamma dose rate by gamma ray field spectrometer. Nucl. Tracks Radiat. Meas. 14, 209.
Sengupta, D., Kumar, R., Singh, A.K., Prasad, R., 2001. Radon exhalation and radiometric prospecting in rocks associated with CuU mineralisations in the Singhbhumshear zone, Bihar. Appl. Rad. Isot. 55, 889.
de Souza e Silva, R., et al., May 3-7, 2009. Object oriented design of anthropomorphic phantoms and GEANT4-based implementations. In: International Conference on Mathematics, Computational Methods and Reactor Physics (M&C 2009) Saratoga Springs, New York.
Sonkawade, R.G., et al., 2008. Natural radioactivity in common building construction and radiation shielding materials. Atmos. Environ. 42, 2254.
Stranden, 1979. Radioactivity of building materials and the gamma radiation in dwellings. Phys. Med. Biol. 24, 921.
Takeuchi, K., Shun-ichi, T., 1985. Point isotropic buildup factors of gamma rays, including bremsstrahlung and annihilation radiation for water, concrete, iron, and lead. Nucl. Sci. Eng. 90, 158.
Trubey, D.K., 1966. A Survey of Empirical Functions Used to Fit Gamma-ray Buildup Factors, ORNL-RSIC-10. http://www.ornl.gov/info/reports/1966/3445600231354.pdf.
Tzortzis, M., Haralabos, T., Christofids, S., Christodoulides, G., 2003. Gamma radiation measurements and dose rates in commercially used natural tiling rocks (granites). J. Environ. Radioactivity 70, 223.
UNSCEAR, 1988. Sources and effects of Ionizing radiation, United Nations Scientific Committee on the effects of Atomic radiation. Sources, Effects and Risk of Ionizing Radiation. United Nations, New York.
UNSCEAR, 1993. Sources and effects of Ionizing radiation, United Nations Scientific Committee on the effects of Atomic radiation. Exposure from Natural Sources of Radiation. United Nations, New York.
UNSCEAR, 2000. Sources and effects of Ionizing radiation, United Nations Scientific Committee on the effects of Atomic radiation. Exposures from Natural Radiation Sources, Annex B. United Nations, New York.
Walley El-Dine, N., El-Shershaby, A., Ahmed, F., Abdel-Haleem, A.S., 2001. Measurement of radioactivity and radon exhalation rate in different kinds of marbles and granites. Appl. Rad. Isot. 55, 853.
Xinwei, L., 2006. Natural radioactivity in some building materials and by-products of Shaanxi, China. J. Radioanal. Nucl. Chem. 267, 669.
Yang, Y., Wu, X., Jiang, Z., Wang, W., Lu, J., Lin, J., Wang, L., Hsia, Y., 2005. Radioactivity concentration in soils of the Xiazhuang granite area, China. Appl. Rad. Isot. 63, 8255.
Zubal, I.G., Harrell, C.R., Smith, E.O., Rattner, Z., Gindi, G., Hoffer, P.B., 1994. Computerized three-dimensional segmented human anatomy. Med. Phys. 21, 299.